Unwrapping Cochlear Implants by Spiral CT

Ge Wang,* *Member, IEEE,* Michael W. Vannier, Margaret W. Skinner, Willi A. Kalender, Arkadiusz Polacin, and Darlene R. Ketten

Abstract— **Multielectrode, intracochlear implants were designed for individuals with profound sensorineural hearing loss who derive little or no benefit from acoustic hearing aids. Determination of each electrode's position in a patient's inner ear may improve speech processor programming to maximize speech recognition. In this paper, an approach is described to use as input a volumetric spiral computed tomography (CT) image of the Nucleus electrode array (Cochlear Pty. Ltd, Lane Cove, NSW, Australia) to unwrap it, and to measure its implanted length given starting and end points. Representative curvilinear structures were digitally synthesized in image volumes of isotropic 0.1-mm voxels. The electrode array was spirally CT-scanned *in vitro* and *in vivo*, and reconstructed on an isotropic grid in 0.1-mm steps. Two algorithms were constructed to track and measure these curvilinear structures. The first algorithm is Karhunen–Loeve (K-L)-transform based, in which the K-L transform is locally applied at a current main axis position to determine the eigenvectors of the main axis voxels, the next main axis position is estimated from the current position along the principal eigendirection, adjusted to the mass center of the orthogonal cross section passing through the estimated position, and then scaled to have a prespecified step. The second algorithm is similar to the first one but avoids use of the K-L transform. In the second algorithm, the next position is directly estimated along the local direction and then processed with the same correction and scaling operations. With user-specified starting and end points as well as a local direction at the starting point, a curvilinear structure can be automatically tracked using either of the algorithms. The first algorithm is more robust, while the second one is more efficient. In the numerical and *in vitro* studies, the lengths of the curvilinear structures were accurately measured. Given local directions determined in the tracking process, an electrode array image can be unwrapped into a linear array with the central electrode axis as the abscissa. The unwrapping approach allows longitudinally and cross-sectionally accurate measurement and better visualization of cochlear implant images. With preimplantation knowledge of length, width, and center electrode distance, the position of individual electrodes can be estimated after unwrapping.**

Manuscript received July 19, 1994; revised March 15, 1996. This work was supported in part by the Whitaker Foundation under the Biomedical Engineering Program and by the National Institutes of Health NIDCD under Grants R03 DC 02798 and R01 DC 00581. *Asterisk indicates corresponding author.*

*G. Wang is with the Mallinckrodt Institute of Radiology, Washington University School of Medicine, Saint Louis, MO, 63110 USA (e-mail: gwang@linda.wustl.edu).

M. W. Vannier is with the Mallinckrodt Institute of Radiology, Washington University School of Medicine, Saint Louis, MO 63110 USA.

M. W. Skinner is with the Department of Otolaryngology-Head and Neck Surgery, Washington University School of Medicine, Saint Louis, MO 63110 USA.

W. A. Kalendar is with the University of Erlangen-Nürnberg, Univ.-Institut für Medizinische Physik, Erlangen, Germany.

A. Polacin is with Siemens AG, Bereich Medizinische Technik, Computer-Tomographie, Erlangen, Germany.

D. R. Ketten is with the Department of Otolaryngology, Harvard School of Medicine, Massachusetts Eye and Ear Infirmary, Boston, MA 02115 USA.

Publisher Item Identifier S 0018-9294(96)06105-8.

I. Introduction

THE human temporal bone contains many submillimeter sized structures that are important for normal function of the middle and inner ear. In individuals with profound sensorineural hearing loss who get little or no benefit from hearing aids, sensory structures that transduce sound energy and primary auditory neurons often have degenerated. Multielectrode, intracochlear implants were designed to stimulate the surviving auditory neurons electrically by implanted electrodes with a diameter of approximately 0.3 to 0.5 mm. These implants assist speech recognition in many individuals. Three multielectrode, intracochlear implant systems are currently in use, including the Nucleus device (Cochlear Pty. Ltd., Lane Cove, NSW, Australia) with which more than 11 000 profoundly deaf individuals have been implanted worldwide. The band configuration of this device's electrodes, the proximity of the electrodes, and the presence of the platinum lead wires makes it relatively difficult to determine the position of each electrode with spiral computed tomography (CT) scans [1]–[7].

In vivo three-dimensional (3-D) CT imaging of the temporal bone is being developed to aid in post-operative assessment of the electrode position [8]–[10]. Spiral CT (also referred to as helical CT) is a recent advance, in which source rotation, patient translation, and data acquisition are continuously and simultaneously conducted [11], [12]. Spiral CT not only accelerates data acquisition, but also permits retrospective reconstruction, which means that any transverse slice can be equally well reconstructed from raw projections. Retrospective reconstruction is particularly desirable in temporal bone imaging, while conventional reconstruction only offers a limited number of reconstructed slices and may miss or distort features of sizes comparable to slice thickness.

X-ray CT image resolution is anisotropic; specifically, the longitudinal resolution is substantially worse than the in-plane resolution. Due to continuous table motion and subsequent interpolation, the section sensitivity profile (SSP) in spiral CT is poorer than the longitudinal detector response function [12]–[14]. An analytic study was recently done to compare the longitudinal bandwidths of the conventional and spiral CT processes [15]–[17]. It was shown that for a given X-ray dose, spiral CT with a small reconstruction interval provides wider bandwidth and thus better longitudinal image resolution than conventional CT. This advantage of spiral CT was also experimentally demonstrated [18].

A preliminary study was recently performed on localization of Nucleus electrodes in the cochlear canal [8]. For a demonstration array coiled in gelatin, there was good agreement in electrode length and interelectrode distance between

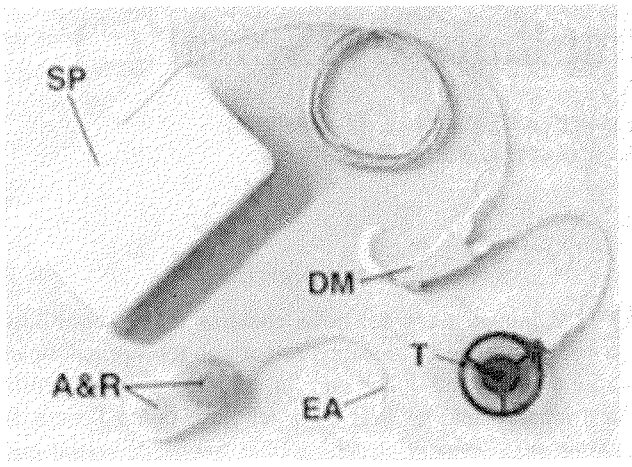

(a)

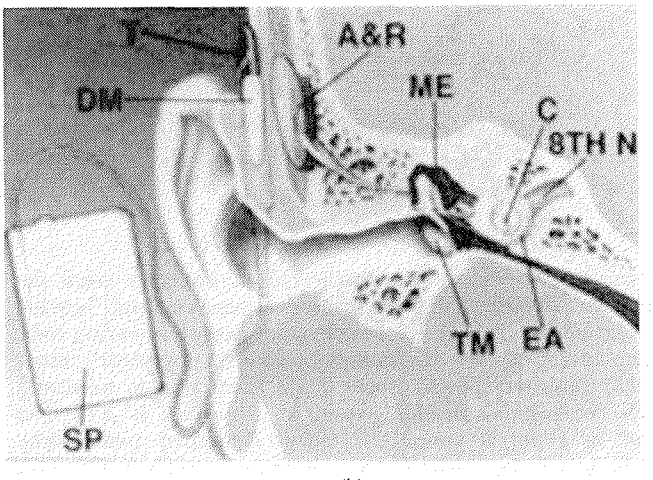

(b)

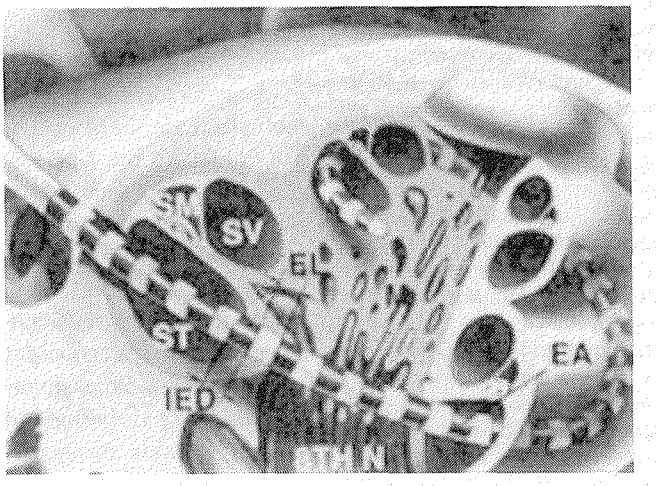

(c)

A&R: Antenna and receiver/stimulator
DM: Directional Microphone EA: Electrode Array
EL: Electrode Length (~0.3 mm)
IED: Inter-Electrode Distance (~0.45 mm)
SP: Speech Processor T: Transmitter
8TH N: EIGHTH NERVE C: COCHLEA
M: MODIOLUS ME: MIDDLE EAR SPACE
SM: SCALA MEDIA ST: SCALA TYMPANI
SV: SCALA VESTIBULI
TM: TYMPANIC MEMBRANE (EARDRUM)

(d)

Fig. 1. Nucleus cochlear implant system (courtesy of Cochlear Corporation, Englewood, CO, USA) and its position after implantation. (a) External parts of the system include a directional microphone, a speech processor, and a transmitter. Internal parts consist of an antenna, a receiver/stimulator, and an electrode array. (b) A temporal bone coronal diagram showing the system in position. (c) A magnified cochlear with an implanted electrode array in position. (d) Abbreviations used in (a), (b), and (c).

measurements with spiral CT and stereo-microscopy, whereas electrode width was increased in CT images mainly due to the partial volume averaging effect. For a cochlear implant patient, the 3-D length of the cochlear canal and the 3-D insertion length of the electrode array were calculated from pre- and post-operative spiral CT scans, respectively. The cross-sectional position of the electrode array in relation to the outer bony wall and modiolus was also measured on several reconstructed images.

Determination of the longitudinal position of each electrode in relation to the total length of a patient's cochlea can be used to estimate the range of acoustic frequencies to which nearby auditory neurons are most sensitive [19]. This information may be important for programming the speech processor to optimize a patient's ability to understand speech. Accurate measurement of the cross-sectional position of each electrode in relation to auditory neurons in the modiolus may also correlate with the behavioral threshold and dynamic range of hearing,

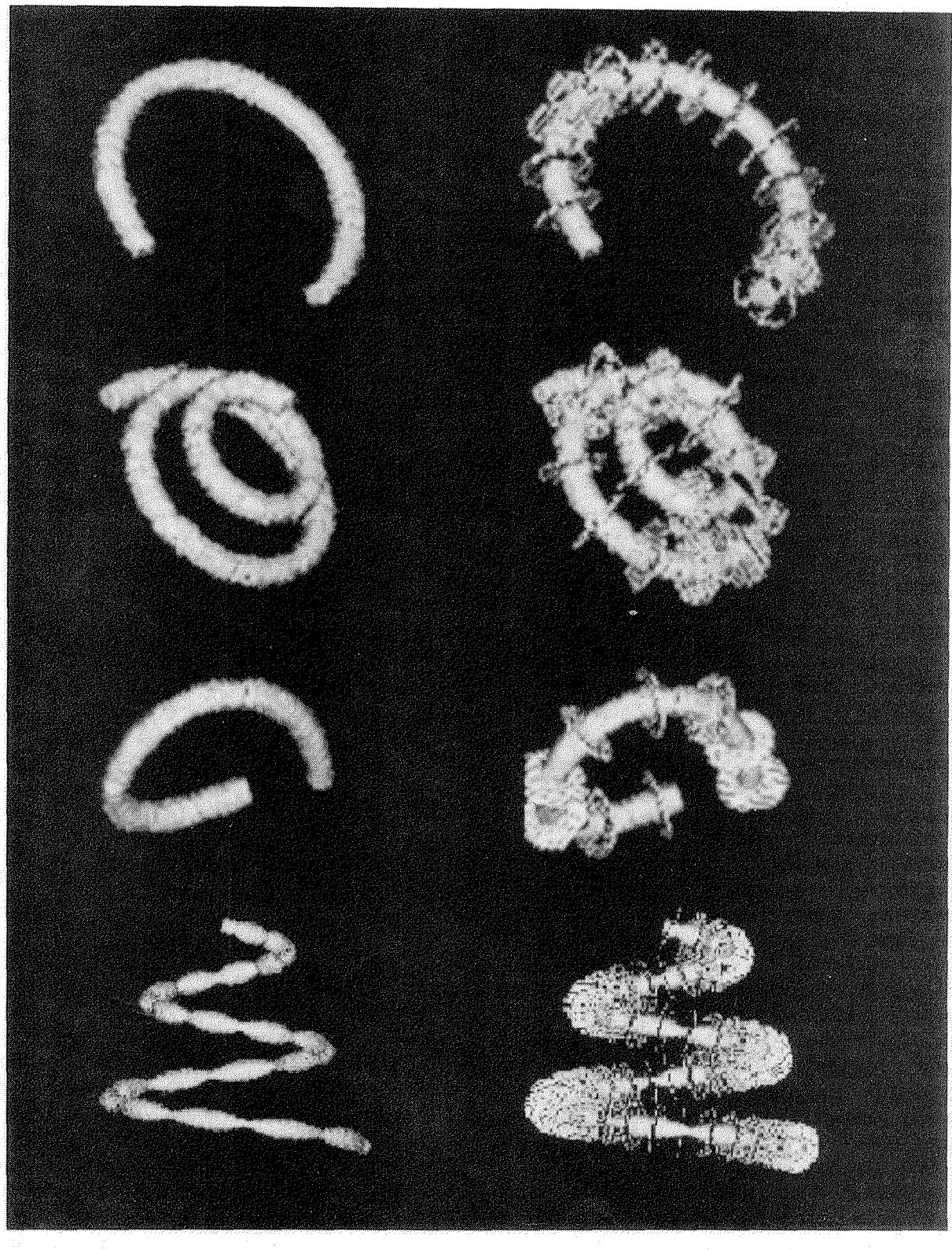

Fig. 2. Surface rendered views of synthetic and tracked C-shaped, spiral, knot, and modulated-spiral structures. The voxel side length is 0.1 mm. Images are 128^3 in the first three rows, and 256^3 in the last row where the cross section radius was sine-modulated with respect to the main axis length. The four curvilinear structures were tracked with steps of 0.4, 0.5, 0.6, and 0.5 mm, respectively. Disks identify orthogonal cross sections separated by four steps.

parameters necessary for programming the speech processor. The purpose of this paper is to demonstrate the feasibility of automatic unwrapping and measurement of the implanted electrode array and neighboring anatomical structures in a spiral CT image to determine the position of individual electrodes. In the unwrapping process, a curvilinear structure is digitally tracked step by step to obtain positional and directional information of its main axis. Subsequently, this information is used to map the structure into an elongated image volume consisting of cross sections orthogonal to the main axis.

II. Materials and Methods

A. Spiral CT Scanner

A spiral CT scanner (Siemens Somatom PLUS-S, Siemens Medical Systems, Iselin, NJ, USA) was employed in this study. This system produces up to 32 consecutive 1-s scans. The detector collimation is selectable from 1 mm to 10 mm. The table increment per gantry rotation varies from 1 to 20 mm. The reconstruction matrix is of 512 by 512 pixels with 4096 gray-levels (12 bits) and an image reconstruction zoom factor up to 16. The maximum in-plane spatial resolution at high contrast is 0.35 mm (at 2%). The cross-field uniformity is ±2 Hounsfield units (HU). A research spiral CT software package was developed on the scanner for opposite neighboring ray interpolation (half-scan interpolation/180LI) [12] and overlapping transverse reconstruction down to 0.1 mm, with a variable gray-level scaling up to a factor of ten to avoid truncation of image voxel values exceeding the conventional maximum (3071 HU).

B. Implant and Data Acquisition

Fig. 1 shows an idealized Nucleus cochlear implant system and its position after implantation. External parts of the system consist of a directional microphone that detects sound and converts it into electronic signals, a speech processor that extracts information from the incoming signal and encodes it into a sequence of data bursts, and a transmitter that sends these bursts through the skin. Internal parts of this system consist of an antenna that detects the data bursts, a receiver/stimulator that decodes them, and an electrode array that causes electrical stimulation of auditory nerve fibers.

A demonstration array was obtained from the manufacturer, which did not meet quality control criteria and was bent during handling. However, the physical features of this array are representative for our purpose and do not affect the conclusions of this feasibility study. This array was measured in three ways. The actual array was placed under a stereomicroscope (Wild, 5A, Switzerland), its dimensions were traced and then measured with a graphic tablet/computer system (Hewlett-Packard, HP-85, Palo Alto, CA, USA). A conventional radiograph was made of the array and measured in the same manner as the actual array. The array was embedded in gelatin, imaged by spiral CT and measured from axial images. The length of the actual array was measured from the silastic tip to the beginning of the coiled lead wires. In addition, an implanted array in an adult patient was scanned five weeks after surgery. In the CT studies, scanning and reconstruction were performed with the gantry tilted to match the Frankfort horizontal, 165 mA for 17 s at 120 kV, 1 mm collimation, 1 mm table increment, 0.1 mm reconstruction interval, 9.8 zoom and the *ultra-high* reconstruction filter. The scale expansion factor used in the *in vitro* and *in vivo* array reconstructions were one and ten, respectively. With these imaging protocols, the scanner was actually operated to maximize the high-contrast image resolution.

Representative curvilinear structures were numerically synthesized into volumetric images of isotropic 0.1 mm voxels.

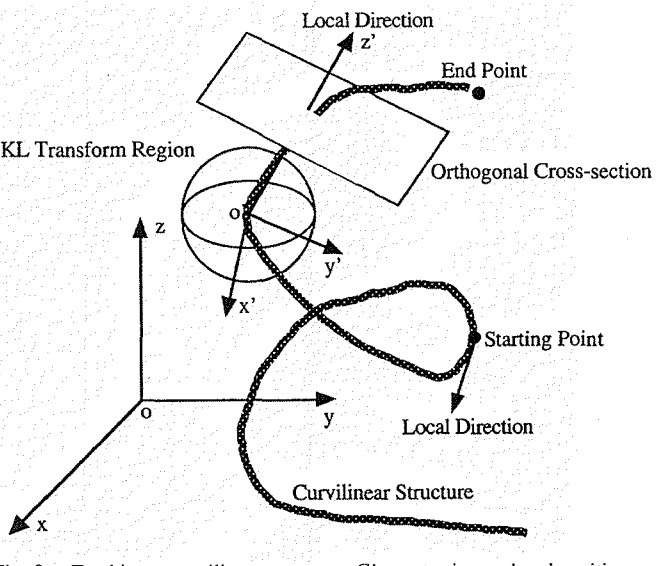

Fig. 3. Tracking a curvilinear structure. Given starting and end positions on the curvilinear structure as well as the local direction at the starting position, the next position can be obtained from the current position along the local direction with either local K-L transformation or direct estimation.

These numerical phantoms are respectively circular, spiral, knot, and sine-modulated spiral segments as shown in the left column of Fig. 2. The synthesis was directly based on well-known mathematical descriptions. For example, the main axis of the sine-modulated spiral phantom is described below

$$\begin{cases} x = 5.12\phi\cos\phi, \\ y = 5.12\phi\sin\phi, \\ z = \frac{179.2(\phi - 2.5\pi)}{4.5\pi} \end{cases} \tag{1}$$

and its cross-sectional radius is modulated as

$$r = \sqrt{10 + 32\sin(10\phi)} \tag{2}$$

where $\phi \in [2.5\pi, 7\pi]$. These formulas were obtained via iterative refinement. The computational unit is in voxel side length. Volumetric images of the phantoms are 128^3 except for the sine-modulated spiral phantom image which is 256^3.

C. Image Unwrapping

Because the linear X-ray absorption coefficient of the platinum electrodes and lead wires is approximately 25 000 HU, the curvilinear structure can be segmented via simple thresholding. In other words, the structure of interest consists of voxels whose HU values are higher than a specified threshold. The streaks generated from the implant have significantly lower HU values than the implant array; therefore, they will not appear after thresholding.

To unwrap a curvilinear structure from user-specified starting to end points, two tracking algorithms were constructed as illustrated in Fig. 3. The flowchart of the unwrapping procedure is given in Fig. 4. The details are explained as follows.

The ANALYZE image analysis and visualization software system [20] was used to specify the starting and end points and a reference direction that will roughly approximate the local direction at this starting point on the main axis of a curvilinear structure. The starting and end points are specified

as follows. The program "Cube Sections" within the ANALYZE interactively generates a simultaneous display of three orthogonal planes of a volumetric image. Each plane can be interactively and independently sliced away in its orientation to reveal interior sections of the volume. The user interface in this program consists of buttons and sliders. Orthogonal slices may be explored with the X, Y, and Z sliders, which are rulers on screen to specify slice indexes with the cursor. The readings of the X, Y, and Z sliders are the coordinates of the intersection point of the orthogonal faces. In clinical practice, the starting point should be selected at the entry of the electrode array into the cochlear canal. The end point should be the tip of the array. The array tip looks like a spherical structure due to partial volume averaging in spiral CT imaging. The X-ray absorption coefficient at its center is approximately 25 000 HU. This center should approximate the tip position reasonably well. With the same program, a reference direction at the starting point can be estimated to approximate the local direction. Because of the imaging protocol we used, the slice thickness was minimized to 1 mm, and the volume averaging effect was accordingly limited. The volume averaging effect will not introduce any significant bias while determining starting and end positions of the array as well as the local direction at the starting point.

The first algorithm is based on the well-known Karhunen–Loeve (K-L) transform [21], [22]. Specifically, consider voxels in a spherical region (Fig. 3) centered at a current position on the curvilinear main axis and of radius R, where R is selected to be substantially larger than the cross-sectional radius r of the curvilinear structure and is also sufficiently small that the linear segment contained in the region of interest (ROI) is approximately straight. A quantitative relationship depends on the curvature and radius of the curvilinear structure under consideration. For example, in our *in vitro* and *in vivo* studies, the radius of the array cross section is about 1 mm, hence R was set to 2 mm. The position vector of a voxel is denoted as $c = (x_i, y_i, z_i), i = 1, 2, \cdots, T$, where T is the total number of the voxels that are within the ROI and have gray-levels higher than a prespecified threshold. The covariance matrix of these voxels is expressed as

$$C_i = \frac{1}{T}\sum_{i=1}^{T}\begin{pmatrix} x_i \\ y_i \\ z_i \end{pmatrix}(x_i \quad y_i \quad z_i) - MM^t \tag{3}$$

where

$$M = \frac{1}{T}\sum_{i=1}^{T}\begin{pmatrix} x_i \\ y_i \\ z_i \end{pmatrix}. \tag{4}$$

C can be transformed to a diagonal C' as follows:

$$C' = \Phi^t C \Phi \tag{5}$$

where

$$C' = \begin{pmatrix} \lambda_1 & & \\ & \lambda_2 & \\ & & \lambda_3 \end{pmatrix}$$

$\lambda_1 \geq \lambda_2 \geq \lambda_3, \Phi = (\phi_1\ \phi_2\ \phi_3), \phi_i = (e_{ix}\ e_{iy}\ e_{iz})^t, i = 1, 2, 3$, are eigenvectors associated with C. The eigenvectors can be directly computed using the K-L transform routines. Geometrically speaking, ϕ_1 approximates the orientation of the linear structure segment and λ_1 is the variance along this direction. From a current main axis position the next main axis position is estimated along the local eigendirection, adjusted to the mass center of the cross section (Fig. 3) orthogonal to the principal eigenvector and passing through the estimated position, and scaled to have a prespecified arc incremental length. The inner product of the principal eigenvector and the reference direction vector is computed to verify if the principal eigendirection is consistent with the reference direction. If the inner product is negative, the principal eigenvector is reversed. Then, the reference direction vector is updated with the principal eigenvector. Tracking continues until the end point is reached.

The second tracking algorithm avoids use of the K-L transform. Given starting and end positions on the main axis of a curvilinear structure as well as the local direction at the starting position, the next position is directly estimated along the local direction, adjusted to the mass center of the cross section (Fig. 3) orthogonal to the local direction and passing through the estimated position, and scaled to have a prespecified arc increment. Then, the new local direction is specified as being from the current position to the next position. The adjustment process may be iterated for higher accuracy.

If a curvilinear structure varies smoothly, the two tracking techniques are essentially equivalent. The second tracking algorithm is computationally more efficient, whereas, the first algorithm is more robust when a thin curvilinear structure contains sharp angles. Specifically, if a current main axis position is at an abrupt turn, the second tracking algorithm may generate an estimated next position that is well off the axis. This misplacement will cause the subsequent mass center adjustment and further tracking to fail.

After the tracking process is finished with either tracking algorithm, the sequence of main axis positions and associated local directions are listed. With this information, cross sections orthogonal to the main axis can be constructed. With the K-L transform based tracking algorithm, the two minor eigenvectors may be used to form a local cross-sectional coordinate system. With the other tracking algorithm, the local directional vector may be cross-multiplied with a proper constant vector to generate a vector orthogonal to the local direction. The two orthogonal vectors are then cross-multiplied to form a vector orthogonal to both. The two orthogonal vectors thus generated can be used to describe the cross section. Appropriate alignment is possible by matching neighboring cross sections. Given the main axis positional and directional information, a curvilinear structure can be readily straightened into a linear array. In the current version of the unwrapping program, nearest neighbor interpolation is used. Nearest neighbor interpolation may be replaced by linear interpolation for more accurate measurements.

The computed total length of a curvilinear structure depends on the tracking step length. If the step is too large, the total

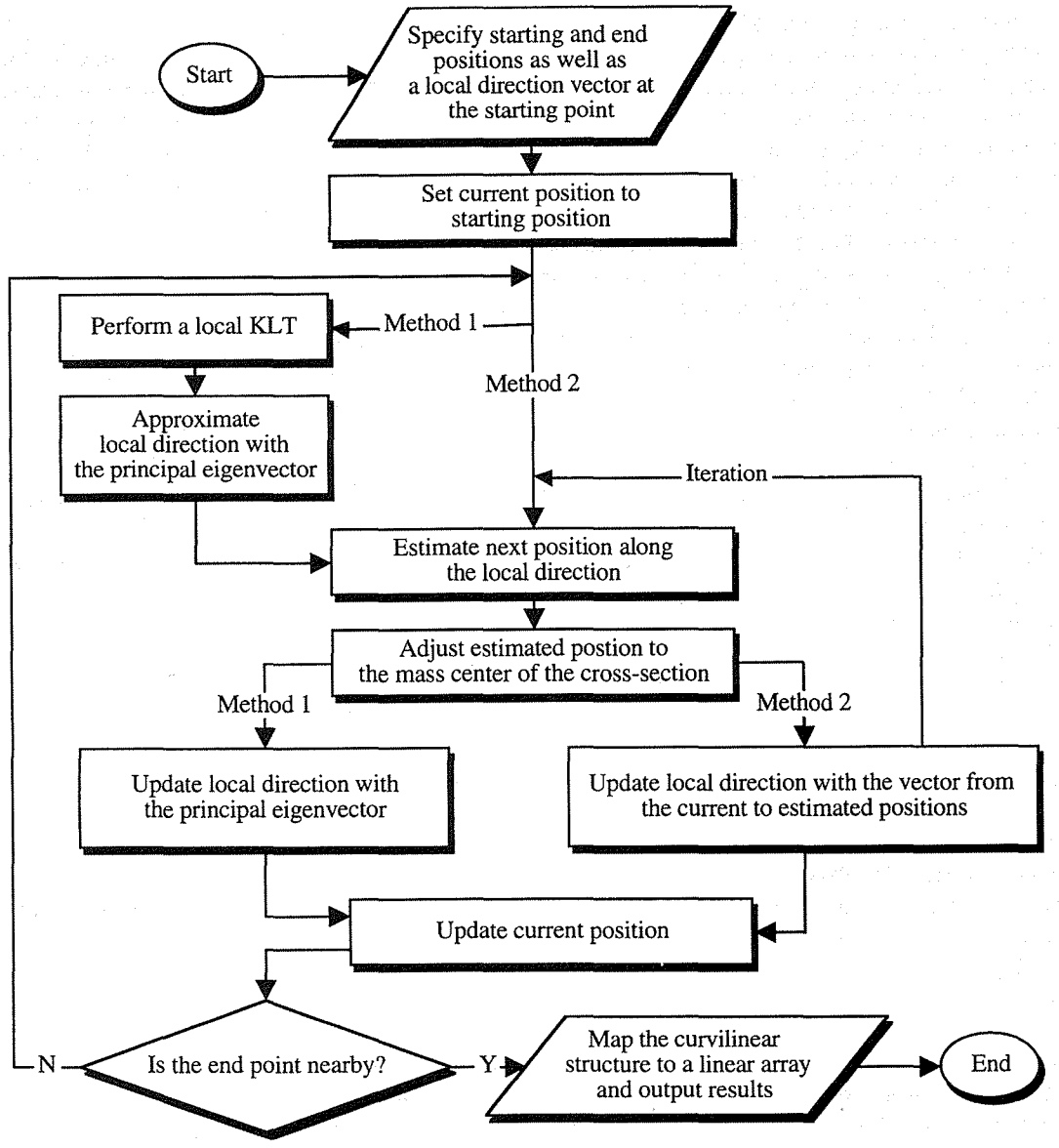

Fig. 4. Flowchart of the unwrapping procedure.

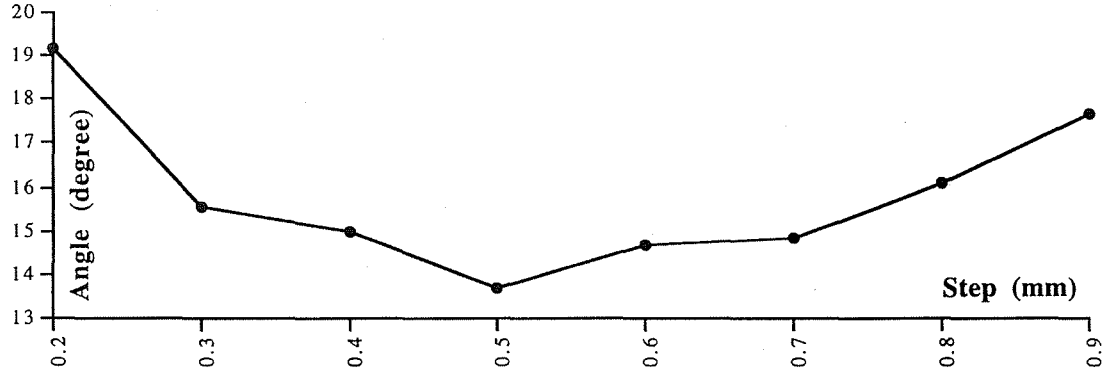

Fig. 5. Average turning angle of the local direction vector as a function of the tracking step. The minimum angle corresponds to the optimal tracking step (0.5 mm).

length will be smaller, because the curvature of the structure cannot be accurately traced. On the other hand, if the step is too small, the total length will be greater, because the inaccuracy in estimating the next main axis position will result in a "zigzag" tracking path. Using the second tracking algorithm, the average turning angle of the local direction vector can be obtained as

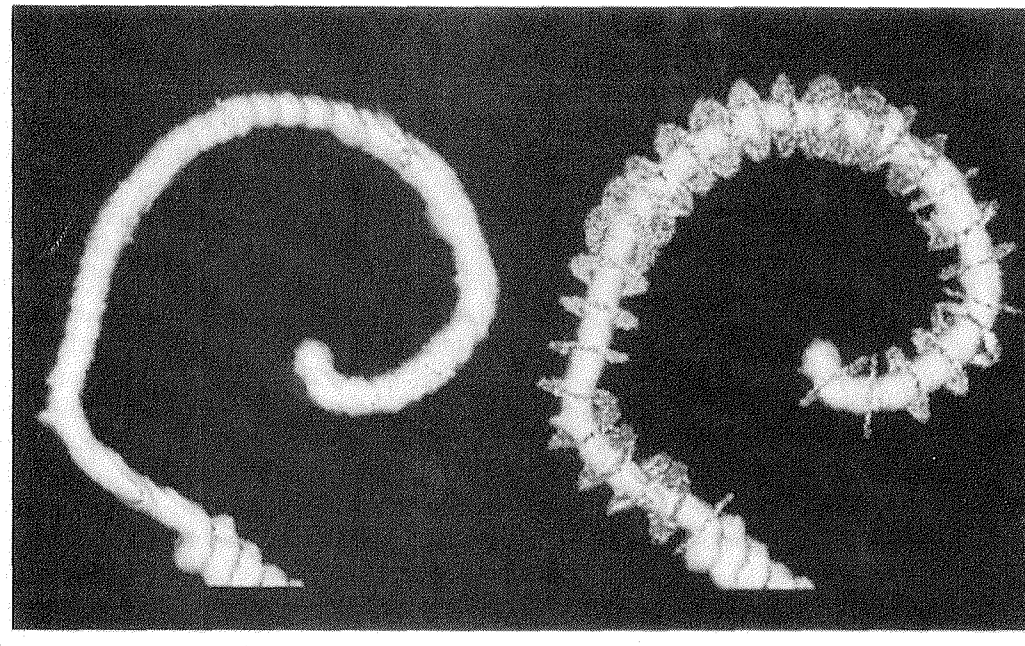

Fig. 6. Surface rendered views of the original and tracked demonstration array thresholded at 800 HU. Disks identify orthogonal cross sections separated by 2 mm.

a function of the tracking step. The optimal tracking step is chosen corresponding to the minimum average turning angle. Fig. 5 shows the average turning angle curve for the spiral phantom (the second row in Fig. 2) where the optimal step should be 0.5 mm. The rationale for the optimal tracking step selection can be explained in the case of a circular curve. Ideally, the average turning angle is directly proportional to the tracking step if it is not too large compared to the radius of the circular curve. Practically, the average turning angle function is U-shaped as a function of the tracking step that is small relative to the curvature radius. When the tracking step is incremented, the average turning angle decreases first, reaches the minimum and then increases. For very small tracking steps, a "zigzag" effect occurs and causes large turning angles. For this reason, these small tracking steps are undesirable. For large tracking steps, approximation of a chord to the arc introduces significant error that causes the total length to be underestimated. Therefore, the tracking step corresponding to the minimum turning angle is preferred.

III. Results

The two tracking algorithms performed similarly in terms of the total length measurement of the curvilinear structures in our experiments. Fig. 2 shows surface rendered views of synthetic and tracked C-shaped, spiral, knot, and sine-modulated-spiral structures before and after tracking using the second algorithm. The voxel side length in all the images is 0.1 mm. The four curvilinear structures were tracked with the optimal steps of 0.4, 0.5, 0.6, and 0.5 mm, respectively. Disks originating from the starting position identify orthogonal cross sections separated by four steps (0.4 mm). This disk separation was arbitrarily selected to illustrate the feasibility of determining orthogonal cross sections. Theoretically, these disks can be placed as densely as needed. The digitally measured total lengths of 20.78, 42.48, 19.98, and 110.1 mm are very consistent to the true values of 20.73, 42.5, 20.0, and 109.9 mm, respectively.

Direct measurement was made of the demonstration array by physically straightening it along a ruler. Its length from the silastic tip to the termination of the coiled lead wire was 57.1 mm. The demonstration array image thresholded at 800 HU was digitally tracked using the second algorithm. The computed total length is 57.8 mm, based on 0.5-mm tracking steps except for the last segment before the end point. The length of the last segment was computed directly. The relative error in this computed measurement is about 1.2%. In the unwrapping process, the array was marked with disks 2 mm apart for visualization. In Fig. 6, 29 disks are shown which are centered at and orthogonal to the array main axis.

An example of a 3-D reconstruction of an *in vivo* implanted array is shown in Fig. 7. Prior to this reconstruction, an image volume of 0.1 mm voxels was reconstructed with ten-fold scale expansion to avoid truncation at the conventional maximum CT number (3071 HU). For Fig. 7, a threshold of 800 HU was used, the implanted array was tracked in 0.5 mm steps using the first algorithm, and then marked with six orthogonal disks 2 mm apart. Subsequently, the slices orthogonal to the longitudinal axis of the implanted array were stacked. Three of these cross-sectional slices are shown in Fig. 8. The slices were displayed with a gray-level range $(-1000, 6000)$ in HU to reveal anatomical structures surrounding the array. However, the choice of an upper limit of 6000 HU caused truncation of the range of HU well below the 25 000 HU of the platinum electrodes and platinum-iridium lead wires. Consequently, the cross-sectional image of the array appears larger than its actual size. However, a raw absorption value profile can be drawn across the diameter of the array image to estimate its size more accurately. Given the manufactureer's specifications of

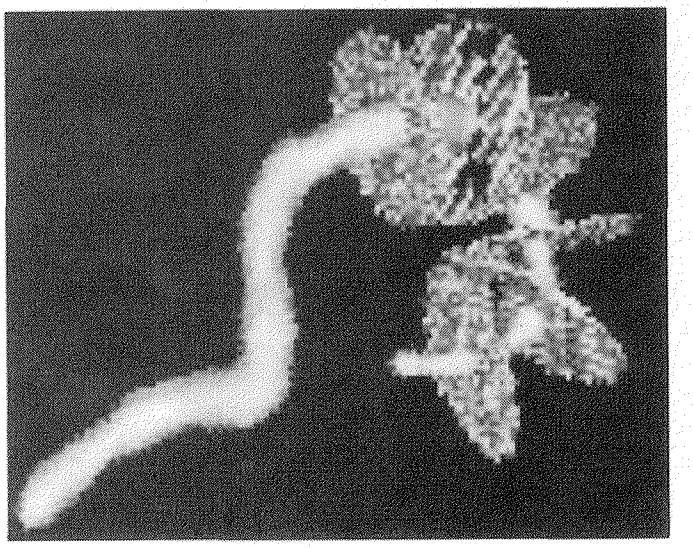

Fig. 7. Surface rendered view of the implanted and tracked array thresholded at 800 HU. Disks mark orthogonal cross sections separated by 2 mm.

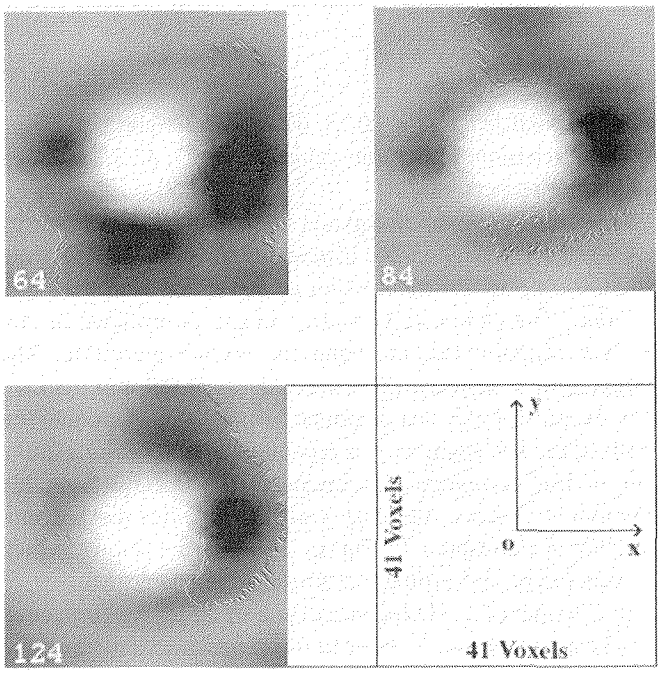

Fig. 8. Cross-sectional images demonstrating the feasibility of unwrapping the cochlear implant array. The images are orthogonal to the array main axis and shown in the range of −1000 HU through 6000 HU. The voxel side length is 0.1 mm. The number on the lower-left corner is the image number indexed along the array axis.

the distribution of electrodes along the array, cross-sectional slices can be placed orthogonal to the array and centered at the approximate longitudinal center of each electrode. With the profile mentioned above, the distance from the cross-sectional center of an electrode to the modiolus and outer bony wall of the cochlea can be estimated.

IV. Discussion

Estimation of the longitudinal and cross-sectional position of each electrode will provide a basis for monitoring possible migration of the array out of the cochlea and may allow better selection of sound processing parameters [23]. Typically, estimation of the electrode position is based on the surgeon's report and on post-operative conventional radiographs [23]–[25]. Estimates of the characteristic frequency range of neurons near the array are determined based on average distributions of the human cochlea and the frequency-position function [19]. Use of this information provides only a rough approximation for two reasons. First, a conventional radiograph does not display the height of the cochlear spiral, a factor essential for accurately determining the cochlear canal length [26]. Second, human cochlear length varies from 28 to 40 mm [27], [28]. For accurate measurement of the longitudinal position of electrodes, values must be obtained from 3-D reconstructions of an individual's inner ear from CT scans [8]. We hypothesize that patients will have better speech recognition if assignment of frequency bands to electrodes in the speech processor is based on 3-D values.

The algorithms we developed for unwrapping a cochlear implant array allows improved measurement of the total implanted length compared to estimates from conventional radiographs. These algorithms also allow visualization of cross sections orthogonal to the longitudinal axis of the array. When these cross sections are placed at the estimated position of each electrode based on the manufacturer's array specification, the distance of the electrode from the modiolus and outer bony wall of the cochlea can be estimated.

Acknowledgment

The authors would like to thank R. L. Yoffie, G. Foster, N. Hente, B. Brunsden, R. Knapp, and R. Walkup for their technical assistance. They also appreciate the ANALYZE software from Dr. R. A. Robb and associates at the Mayo Biomedical Imaging Resource, Rochester, MN. We are also grateful to reviewers for their valuable comments.

References

[1] G. M. Clark, P. J. Blamey, A. M. Brown, P. A. Busby, R. C. Dowell, B. K.-H. Franz, B. C. Pyman, R. K. Shepherd, Y. C. Tong, R. L. Webb, M. S. Hirshorn, J. Kuzma, D. J. Mechlenburg, D. K. Money, J. F. Patrick, and P. M. Seligman, "The University of Melbourne—Nucleus multi-electrode cochlear implant," *Adv. Oto-Rhino-Laryngol.*, vol. 38, pp. 1–189, 1987.

[2] M. F. Dorman, K. Dankowski, G. McCandless, J. L. Parkin, and L. Smith, "Longitudinal changes in word recognition by patients who use the ineraid cochlear implant," *Ear Hear*, vol. 11, pp. 455–459, 1990.

[3] M. W. Skinner, L. K. Holden, T. A. Holden, R. C. Dowell, P. M. Seligman, J. A. Brimacombe, and A. L. Beiter, "Performance of postlinguistically deaf adults with the Wearable Speech Processor (WSP III) and Mini Speech Processor (MSP) of the nucleus multi-electrode cochlear implant," *Ear Hear*, vol. 12, pp. 3–22, 1991.

[4] M. J. Osberger, R. T. Miyamoto, S. Zimmerman-Phillips, J. L. Kemink, B. S. Stroer, J. B. Firszt, and M. A. Novak, "Independent evaluation of the speech perception abilities of children with the nucleus 22-channel cochlear implant system," *Ear Hear*, vol. 12 (4, suppl.), pp. 66–80, 1991.

[5] R. A. Schindler and D. A. Kessler, "Preliminary results with the Clarion cochlear implant," *Laryngoscope*, vol. 102, pp. 1006–1013, 1992.

[6] N. Tye-Murray, R. S. Tyler, G. Woodworth, and B. J. Gantz, "Performance over time with a nucleus or ineraid cochlear implant," *Ear Hear*, vol. 13, pp. 200–209, 1992.

[7] K. Dankowski, *Ineraid Audiologist's Manual*. Bartlett, TN: Smith and Nephew Richards, 1992.

[8] M. W. Skinner, D. R. Ketten, M. W. Vannier, G. A. Gates, R. L. Yoffie, and W. A. Kalender, "Determination of the position of nucleus implant electrodes in the inner ear," *Amer. J. Otol.*, Sept. 1994.
[9] K. Kimura and S. Koga, Eds. *Basic Principles and Clinical Applications of Helical Scan—Applications of Continuous-Rotation CT.* Tokyo: Iryokagakusha, 1994.
[10] M. W. Vannier and G. Wang, "Spiral CT refines temporal bone imaging," *Diagnost. Imag.*, vol. 15, pp. 116–121, 1993.
[11] W. A. Kalender, W. Seissler, E. Klotz, and P. Vock, "Spiral volumetric CT with single-breath-hold technique, continuous transport, and continuous scanner rotation," *Radiol.*, vol. 176, pp. 181–183, 1990.
[12] C. R. Crawford and K. F. King, "Computed tomography scanning with simultaneous patient translation," *Med. Phys.*, vol. 17, pp. 967–982, 1990.
[13] W. A. Kalender and A. Polacin, "Physical performance characteristics of spiral CT scanning," *Med. Phys.*, vol. 18, pp. 910–915, 1991.
[14] J. A. Brink, J. P. Heiken, D. M. Balfe, S. S. Sagel, J. DiCroce, and M. W. Vannier, "Spiral CT: Decreased spatial resolution *in vivo* due to broadening of section-sensitivity profile," *Radiol.*, vol. 185, pp. 469–474, 1992.
[15] G. Wang and M. W. Vannier, "Spatial variation of section sensitivity profile in helical CT," *Med. Phys.*, vol. 21, pp. 1491–1497, 1994.
[16] ——, "Longitudinal resolution in volumetric X-ray CT—Analytical comparison between conventional and helical CT," *Med. Phys.*, vol. 21, pp. 429–433, 1994.
[17] G. Wang, J. A. Brink, and M. W. Vannier, "Theoretical FWTM values in helical CT," *Med. Phys.*, vol. 21, pp. 753–754, 1994.
[18] W. A. Kalender, A. Polacin, and C. Suss, "A comparison of conventional and spiral CT: An experimental study on the detection of spherical lesions," *J. Comput. Assist. Tomogr.*, vol. 18, pp. 167–176, 1994.
[19] D. D. Greenwood, "A cochlear frequency-position function for several species—29 years later," *J. Acoust. Soc. Amer.*, vol. 87, pp. 2595–2605, 1990.
[20] R. A. Robb *et al.*, *ANALYZE™ Reference Manual*, Version 6.2, Biomedical Imaging Resource, Mayo Foundation, 1993.
[21] H. Karhunen, English translation by I. Selin, *On Linear Methods in Probability Theory*, The Rand Corporation, Doc. T-131, Aug. 11, 1960.
[22] R. M. Haralick and L. G. Shapiro, *Computer and Robot Vision, Volume II.* Reading, MA: Addison-Wesley, 1993.
[23] L. A. Whitford, P. M. Seligman, P. J. Blamey, H. J. McDermott, and J. F. Patrick, "Comparison of current speech coding strategies," *Adv. Otorhinolaryngol.*, vol. 48, pp. 85–90, 1993.
[24] R. T. Miyamoto and H. E. Maddox III, "Medical and surgical issues," *Amer. J. Otol.*, vol. 12 (suppl.), pp. 18–21, 1991.
[25] M. A. Marsh, J. Xu, P. J. Blamey, L. A. Whitford, S. A. Xu, J. M. Silverman, and G. M. Clark, "Radiologic evaluation of multichannel intracochlear implant insertion depth," (an erratum in *Amer. J. Otol.*, vol. 14, p. 627, 1993), *Amer. J. Otol.*, vol. 14, pp. 386–391, 1993.
[26] D. R. Ketten and D. Wartzok, "Three-dimensional reconstruction of the dolphin ear," in *Sensory Abilities of Cetaceans: Field and Laboratory Evidence*, J. Thomas and R Kastelein, Eds. New York: Plenum. Also in *Proc. NOTA ASI Ser. A, Life Sci.*, 1990, vol. 196, pp. 81–105.
[27] M. Hardy, "The length of the organ of Corti in man," *Amer. J. Anat.* vol. 62, pp. 291–311, 1938.
[28] L. Ulehlova, L. Voldrich, and R. Janisch, "Correlative study of sensory cell density and cochlear length in humans," *Hearing Res.*, vol. 28, pp. 149–151, 1987.

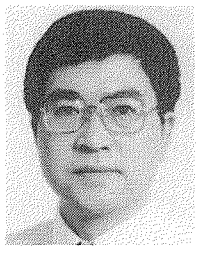

Ge Wang (S'90–M'92) received the B.Eng. degree in electrical engineering at Xidian University, Xian, China, in 1982, the M.S. degree in remote sensing at Graduate School of Academia Sinica, Beijing, China, in 1985, and M.S. and Ph.D. degrees in electrical and computer engineering at State University of New York, Buffalo, NY, in 1991 and 1992, respectively.

He worked as Instructor and Assistant Professor at Department of Electrical Engineering, Graduate School of Academia Sinica from 1984 to 1988. Currently, he is Assistant Professor at Mallinckrodt Institute of Radiology, Washington University, St. Louis, MO. His research interests are computed tomography and image analysis, with emphasis on spiral/helical CT. He has authored over 40 peer-reviewed and invited publications.

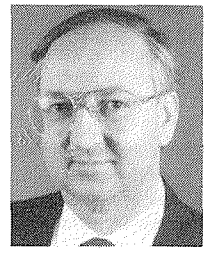

Michael W. Vannier graduated from the University of Kentucky School of Medicine and completed a diagnostic radiology residency at the Mallinckrodt Institute of Radiology, Washington University School of Medicine, St. Louis, MO. He holds degrees in engineering from University of Kentucky, Lexington, and Colorado State University, Fort Collins, and was a student at Harvard University and the Massachusetts Institute of Technology, Cambridge, MA.

He is Professor at the Mallinckrodt Institute of Radiology. His primary research interests are morphometry and anthropometry based on volumetric imaging modalities, especially CT, MR, and PET/SPECT.

Dr. Vannier has authored more than 250 scientific publications and serves as Editor-in-Chief of the IEEE TRANSACTIONS ON MEDICAL IMAGING. In 1994, he was inducted in the U.S. Space Foundation Hall of Fame for work on digital medical imaging.

Margaret W. Skinner received the B.A. degree in chemistry from Wellesley College, Wellsley, MA, the M.A. degree in audiology from Case-Western Reserve University, Cleveland, OH, and the Ph.D. degree in audiology from Washington University, St. Louis, MO.

She is an Audiologist in the Department of Otolaryngology-Head & Neck Surgery, Washington University School of Medicine, St. Louis, MO, where she is Associate Professor, Director of Audiology, and Director of the Cochlear Implant Program.

Her classic book, *Hearing Aid Evaluation*, (Englewood Cliffs, NJ: Prentice-Hall, 1988) integrates her broad clinical experience with her research on what hearing aid characteristics provide hearing-impaired individuals with optimized speech recognition. In her current research, she examines what speech coding strategies and speech processing parameters will provide profoundly deaf adults implanted with multielectrode, intracochlear implants with the best opportunity to recognize speech. Knowledge of electrode position in the inner ear may prove important in the selection of coding strategy and processing parameters. She has authored 40 publications in peer-reviewed journals or books.

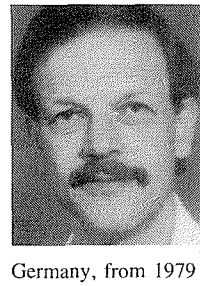

Willi A. Kalender finished study in physics at Bonn University, Bonn, Germany, in 1973, and received the M.S. and Ph.D. degrees in medical physics at University of Wisconsin, Madison, in 1974 and 1979, respectively.

He was tenured in Medical Physics at Tubingen University, Tubingen, Germany, in 1988. He has worked as Research Assistant at Siemens Corporate Research from 1976 to 1979, and as a Leader of Medical Physics Group in Computed Tomography Department of Siemens Medical Systems, Erlangen, Germany, from 1979 to 1995. He is currently Head of Institute for Medical Physics of Friedrich-Alexander University, Erlangen-Nüernberg, Germany. His research area is medical physics with special emphasis on computed tomography. He has authored over 300 publications and several patents.

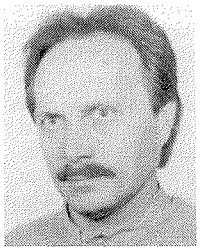

Arkadiusz Polacin finished the B.Eng. and M.S. degrees in electrical and computer engineering at Warsaw University of Technology, Warsaw, Poland, in 1981 and received the Ph.D. degree in computer engineering at Warsaw University of Technology in 1986.

He has worked as Research Assistant from 1981 to 1986 and as Assistant Professor from 1987 to 1989 in Department of Nuclear and Medical Electronics, Electronics Faculty of Warsaw University of Technology. Since 1989 he is with Medical Physics Group of Siemens Medical Systems, Erlangen, Germany. He has published over 50 scientific papers and has two patents on medical imaging. His main research topic is computed tomography. Additionally he is dealing with signal/image processing and multiprocessor systems.

Darlene R. Ketten received the B.A. degrees in biology and French from Washington University, St. Louis, MO, the M.S. degree in oceanography from Massachusetts Institute of Technology, Cambridge, and the Ph.D. degree jointly awarded in neuroanatomy and experimental radiology from the Johns Hopkins University and Johns Hopkins Medical Institution, Baltimore, MD.

She is a Marine Biologist and Neuroanatomist in the Department of Otology and Laryngology, Harvard Medical School, Cambridge, MA, where she is Assistant Professor, Research Director of the Three-Dimensional Head and Neck Imaging Service, and Co-investigator in the Cochlear Implant Research Laboratory. She has developed three-dimensional techniques for analyzing placement of inner ear implants *in vivo*. Her current research is focused on three-dimensional anatomical models of the inner ear, based on histology and computed tomography, that are used to analyze how structural differences in different species and different pathologies affect hearing abilities. She has authored over 50 publications in peer-reviewed journals.